ROYAL SOCIETY
OF CHEMISTRY

PAPER

Check for updates

Reconfigurable assembly of charged polymer-modified Janus and non-Janus particles: from half-raspberries to colloidal clusters and chains†

Claudia Marschelke, [ab] Olga Diring[ab] and Alla Synytska (ID) *[ab]

Understanding the dynamic and reversible assembly of colloids and particles into complex constructs, inspired by natural phenomena, is of fundamental significance for the fabrication of multi-scale responsive and reconfigurable materials. In this work, we investigate the pH-triggered and reconfigurable assembly of structures composed of binary mixtures of oppositely charged polyacrylic acid (PAA)-modified non-Janus and poly(2-dimethylamino)ethyl methacrylate (PDMAEMA)/poly(*N*-isopropylacrylamide) (PNIPAM)-modified Janus particles driven by electrostatic interactions. Three different target structures are visible both in dispersions and in dry state: half-raspberry structures, colloidal clusters and colloidal chains depending on the mass, numerical and particle size ratio. All formed structures are well-defined and stable in a certain pH range. Half-raspberry-like structures are obtained at pH 6 and numerical ratios $N_{JP/PAA-HP}$ of 1 : 500 (for 200-PAA-HP), 1 : 44 (for 450-PAA-HP) and 1 : 15 (for 650-PAA-HP), respectively, due to electrostatic interactions between the central JP and the excessive PAA-HP. Colloidal chains and cluster-like structures are generated at numerical ratios $N_{JP/PAA-HP}$ of 4 : 5 (for 200-PAA-HP), 4 : 3 (for 450-PAA-HP), and 4 : 1 (for 650-PAA-HP). Moreover, the smaller the size of a "connecting" PAA colloid, the larger is the average length of a colloidal chain. Depending on the particle size ratio $S_{JP/PAA-HP}$, some of the observed structures can be disassembled on demand by changing the pH value either close to the IEP of the PDMAEMA (for half-raspberries) or PAA (for colloidal clusters and chains) and then reassembled into new stable structures many times. The obtained results open a pathway to pH-controlled reconfigurable assembly of a binary mixture composed of polymeric-modified non-Janus and Janus particles, which allow the reuse of particle building blocks.

Introduction

Self-assembly is the basic concept whereby complex structures in nature are formed and it comprises all dimensions, starting from the atomic or molecular level, to cellular processes, phenomena of ethology, and cosmic formations such as solar systems and galaxies. In this context, the internal dynamics in nature are a source of inspiration to form controllable and reversible assembly structures using artificial building blocks such as colloidal particles with a rich functionality of the individual particles, and can serve the development of novel materials for the application in micromotors,[1–3] photonics/plasmonics,[4] drug delivery,[5] catalysis,[6] solar cells,[7] sensors,[8] and electronic ink technology.[9]

The assembly process can be triggered, on the one hand, by the intrinsic properties of the colloids such as charges,[10–14] amphiphilicity[15] and depletion interactions[16,17] forming supra-particular assemblies. On the other hand, assembly can be provoked field-assisted by an electric,[1,18–20] magnetic[21–25] or flow field.[26,27] Assemblies of chemically and geometrically isotropic building blocks typically lead to symmetric structures, while colloids with chemical and/or geometrical anisotropies, such as Janus particles, can assemble into more sophisticated, asymmetric structures depending on the mutual orientation.[10,11] Taking advantage of their chemically anisotropic structure, the assembly of Janus particles can lead to a variety of structures which are inaccessible to their homogeneous counterparts.

Static self-assembly, which was already intensively studied for non-Janus[20,28] and Janus particles,[10,11,26,29,30] comprises thermodynamically stable systems in an equilibrium state.[31,32] Once these static assemblies are formed, the structures are irreversible.

In contrast to that, dynamic systems include non-equilibrium structures which can be reversibly changed by energy input or an external stimulus including pH, light, and temperature.[31,32] Thus, the variation of a chosen parameter or

[a]Leibniz Institute of Polymer Research Dresden e. V., Hohe Straße 6, 01069 Dresden, Germany. E-mail: synytska@ipfdd.de

[b]Dresden University of Technology, Faculty of Mathematics and Science, Institute of Physical Chemistry and Polymer Physics, 01062 Dresden, Germany

† Electronic supplementary information (ESI) available. See DOI: 10.1039/c9na00522f

stimulus accomplishes a programmable adaption of the system. This adaptation is reversible upon the removal of the stimulus. Programmed and especially dynamic assemblies of particles and colloids are of importance for fundamental research and offer great potential for understanding of natural sensory processes and their application-oriented imitation.

Nevertheless, there are only few examples of reversible self-assembly of non-Janus[12,14,27,33–44] and Janus particles[15,25,34,45] discussed in the literature. The reported colloidal building blocks exhibit either a purely soft (organic),[14] purely hard (inorganic), or hybrid (soft/hard) character.[43] An example for dynamic assemblies of soft colloids was shown by Crassous and coworkers who employed oppositely charged temperature-responsive core–shell particles with complementary shapes for a reversible lock-and-key assembly mechanism.[14] Comprehensive studies towards the dynamic self-assembly of soft[15,46] as well as hard Janus particles[1,2,23,25,29,47,48] were performed by Granick *et al.* Already in 2011, they studied the kinetic pathways of self-assembly of sulfate polystyrene Janus particles that were made hydrophobic on one hemisphere through successive deposition of titanium and gold thin films, onto which mono-layers of *n*-octadecanethiol were formed.[15] They showed that at very low salt concentrations (3.8 mM NaCl), particles repel each other due to electrostatic forces, whereas an increase of the ionic strength weakens the repulsive interactions causing triple helix growth by face-sharing tetrahedral. Later, the group of Granick also investigated the impact of magnetic fields on the assembly of hard half-nickel-coated silica Janus particles.[25] By applying a rotating magnetic field of moderate strength, the Janus particles arrange perpendicularly to the field and form hexagonal rotating crystals. Increase of the magnetic field strength causes disaggregation of the crystals into dumbbell-like particle assemblies. In 2016, Velev and co-workers described a thermoresponsive system consisting of polystyrene/iron oxide latex Janus particles.[45] The iron oxide-coated patches are selectively wetted with liquid lipids, driving the particle assembly into colloidal clusters above the phase transition temperature *via* inter-particle capillary bridges. Temperature decrease causes the fluid-to-gel transition of the liquid lipids and subsequent the disassembly of the clusters due to the loss of the capillary forces. Dynamic interactions can also originate from UV-induced switches, as shown by Ren *et al.* who designed SiO$_2$–Pt Janus catalytic micromotors functionalized with spiropyran moieties[49] self-assemble into multiple motors due to electrostatic interactions and π–π stacking induced by UV light irradiation, and disassemble into single motors when the light is switched to green. Recently, Kraft *et al.* demonstrated the potential of non-Janus colloidal joints with controlled stiffness and motion range by assembling them into flexible colloidal chains (called "colloidal polymers") and clusters (called "colloidal molecules").[43]

The aforementioned examples concern the utilization of either soft latex particles or hard/stiff silica particles, which were partly coated with metals or low-molecular compounds. However, to the best of our knowledge, no reports on the programmable and reconfigurable assembly of organic–inorganic polymer-modified colloidal systems are presented in the literature. These systems are especially attractive due to their broadened diversity of functionalities coming from the polymeric shells in terms of their chemical design and responsiveness to pH, ionic strength, UV light or temperature[12] as well as adaptivity. The polymer coating may also impact the kinetics of reversibility of transitions between different structures due to interdiffusion and interpenetration of the polymeric chains. However, stimuli-responsiveness of hairy Janus particles was solely used for the initiation of self-assembly processes,[10,11] while switchability of these assemblies caused by changes of ambient parameters remained challenging and has not been investigated yet.

Here, we report on the reconfigurable assembly of structures composed of binary mixtures of poly(2-dimethylamino)ethyl methacrylate (PDMAEMA)/poly(*N*-isopropylacrylamide) (PNIPAM) Janus and polyacrylic acid (PAA)-decorated non-Janus particles. The particles assemble either in half-raspberry-like structures, colloidal clusters or colloidal chains depending on the particle size ratio $S_{\text{JP/PAA-HP}}$ and mass ratio $M_{\text{JP/PAA-HP}}$ as well as numerical ratio $N_{\text{JP/PAA-HP}}$. The formed structures are well-defined and stable in a certain pH range. Some of the structures also have the advantage that the particle interactions are bistable. They can be disassembled on demand by changing the pH value, and then reassembled into new stable structures many times.

Experimental section

Materials and methods

Materials. Tetraethylorthosilicate (TEOS, Fluka, 99%), ammonium hydroxide (NH$_4$OH, Acros Organics, 28–30% solution), ethanol abs. (EtOH, VWR, 99.9%), 3-amino-propyltriethoxysilane (APTES, ABCR, 97%), α-bromoisobutyryl bromide (Aldrich, 98%), α-bromoisobutyric acid (Aldrich, 98%), anhydrous dichloromethane (Acros Organics, 99.8%), triethyl-amine (99%, Sigma-Aldrich), fluorescein isothiocyanate (isomer I, ≥90%, Sigma), rhodamine B isothiocyanate (mixed isomers, BioReagent, Aldrich), copper(II) bromide (Aldrich, 99.999%), tin(II) 2-ethylhexanoate (Aldrich, 95%), tris(2-pyridylmethyl) amine (TPMA, Aldrich, 98%), *N,N,N′,N″,N″*-penta-methyldiethylenetriamine (PMDTA, Aldrich, 99%), anhydrous *N,N*-dimethylformamide (DMF, Sigma-Aldrich, 99.8%), ethyl α-bromoisobutyrate (EBiB, Aldrich, 98%), toluene (Sigma-Aldrich, 99.8%), chloroform (Sigma-Aldrich, 99.5%), hydrochloric acid (Sigma, 36.5–38.0%), methanesulfonic acid (Sigma-Aldrich, 99.5%), sodium hydroxide (NaOH, pellets, Sigma-Aldrich, 97%), diethyl ether (Aldrich, 99.7%), paraffin wax (mp 53–57 °C, Aldrich), *N*-(3-dimethylaminopropyl)-*N′*-ethylcarbodiimide hydrochloride (EDC, Sigma-Aldrich), *N*-hydroxysuccinimide (NHS, Aldrich, 98%), dichloromethane (Acros Organics, 99.99%), hexane (Sigma-Aldrich, 95%), and carboxy-terminated poly(*N*-isopropylacrylamide) (PNIPAM, M_n: 62 kg mol^{-1}; Polymer Source) were used as received. *Tert*-butyl acrylate (*t*BA, Aldrich, 98%) and 2-(dimethylamino)ethyl methacrylate (DMAEMA, Aldrich, 98%) were passed prior to the polymerization through basic, neutral, and acidic aluminum oxides. Millipore water was obtained from Milli-Q (Millipore, conductivity: 0.055 μS cm^{-1}).

Scanning electron microscopy (SEM). Scanning electron microscopy (SEM) images were acquired on a NEON 40 EsB CrossBeam scanning electron microscope (Carl Zeiss NTS GmbH, Germany), operating at 3 keV in the secondary electron and InLens mode. In order to enhance electron density contrast, samples were coated with platinum (3.5 nm) using a Leica EM SCD500 sputter coater.

Dynamic light scattering measurements (DLS). Zetasizer Nano ZS (Malvern Instruments, UK) was used for the determination of the particle size (hydrodynamic diameter) using plastic cells for aqueous suspensions. The device is equipped with a 633 nm laser and with a non-invasive backscatter (NIBS) technology for increasing the particle size sensitivity.

Electrokinetic measurements. The pH-dependent electrokinetic (zeta potential) measurements of the particles in suspension were carried out with a Zetasizer Nano ZS (Malvern Instruments, UK) and an MPT-2 autotitrator. For all the measurements, the particles were suspended in a 10^{-3} M KCl solution in water. The pH of the prepared suspensions was controlled by adding 0.1 M KOH or HCl aqueous solutions. Three measurements were recorded for each sample at each pH value.

Thermogravimetric analysis (TGA). Thermogravimetric analysis was performed to measure the polymer layer thickness on the particle surface. All measurements were conducted in air atmosphere on a TGA Q 5000IR analyzer (TA Instruments, USA). The thickness of the grafted layer on SiO_2 particles was determined by the equations described elsewhere.[50]

Fluorescence microscopy (FLM). The fluorescence microscopy images were acquired on a *Dragonfly* spinning disk confocal microscope (Andor – Oxford Instruments) using a 100x immersion oil objective (Carl Zeiss Microscopy GmbH, Germany). For data acquisition, a FITC (excitation: 488 nm; emission: 525/50 nm), and TRITC (excitation: 561 nm; emission: 600/50 nm) filter set in conjunction with a *iXon EMCCD* camera and the *Imaris* image processing program were used.

Synthesis of spherical SiO_2-based non-Janus and Janus particles

Synthesis and pre-modification of monodisperse silica particles. 200–1000 nm silica particles were synthesized using a multistep hydrolysis-condensation procedure of TEOS in an ammonia hydroxide–ethanol solution based on the Stöber approach, and described in ref. 51. In brief, TEOS was added sequentially into a mixture of ethanol and ammonia solution. The particles produced within one step of the synthesis were used as seeds for the next step. Each reaction was carried out by stirring the mixture at 500 rpm overnight at room temperature (starting from the last addition of TEOS). Subsequently, the dispersion with particles of the desired size was separated from the solvent by centrifugation, yielding monodisperse silica spheres. Rhodamine B isothiocyanate or fluorescein isothiocyanate were added during the preparation of these particles in order to label the resulting particles with a red or green fluorescent dye. Purified particles were dried in a vacuum oven at 60 °C and then modified with (3-aminopropyl)triethoxysilane

(APTES) to introduce amino groups onto the surface. This was achieved by stirring the particles for 24 hours in a 5 vol% APTES solution in ethanol. The particles were then purified by repeated washing and centrifugation cycles in ethanol, and dried at 60 °C. Afterwards, the ATRP-initiator (α-bromoisobutyryl bromide) was immobilized onto the surface of the dried amino-modified particles. For this purpose, 1000 mg of the particles were dispersed in 35 mL of anhydrous dichloromethane, followed by the addition of 1.4 mL triethylamine and 0.7 mL α-bromoisobutyryl bromide. The reaction was carried out at room temperature under constant stirring for 2 hours. The modified particles were purified by repeated washing and centrifugation cycles in ethanol, and dried under reduced pressure at 60 °C.

Grafting of PDMAEMA, and PtBA using surface-initiated ATRP. Poly(2-dimethylaminoethyl methacrylate) (PDMAEMA) was grafted on the ATRP-initiator-modified particles as follows: 3 mL anhydrous DMF, 30 μL $CuBr_2$ (0.1 M solution in DMF), 6.5 mg TPMA, 0.15 μL EBiB, and 3 mL DMAEMA were added to a test tube containing initiator-modified green-fluorescent silica particles (200 mg). The test tube was sealed with a rubber septum and purged with argon, 100 μL of Sn(ɪɪ)-2-ethylhexanoate and 1 mL anhydrous DMF were injected. The polymerization was carried out under continuous stirring at 70 °C in a water bath for 40 minutes. Particles with the grafted polymer were washed by centrifugation in DMF and ethanol eight times, and dried under reduced pressure at 25 °C.

A similar procedure was used for the grafting of PtBA on 200 nm, 450 nm, and 650 nm initiator-modified silica particles. For the polymerization, 70 μL PMDTA (0.5 M in DMF), 3 mL *t*BA, 70 μL $CuBr_2$ (0.1 M solution in DMF), and 0.15 μL ethyl α-bromoisobutyrate (EBiB) were added to the red-fluorescent particles. The mixture was sonicated and purged with Ar, followed by the injection of 150 μL of Sn(ɪɪ)-2-ethylhexanoate. The polymerization was performed under continuous stirring at 110 °C for 15 minutes. After the particles were purified by centrifugation and redispersion cycles in toluene and dried, hydrolysis was performed to yield polyacrylic acid (PAA). Briefly, PtBA-covered particles were suspended in 10 mL chloroform in a Teflon centrifuge vial, accompanied by adding 4 mL of methanesulfonic acid and rapidly stirring the mixture for five minutes. The modified particles were collected by diluting the mixture with diethyl ether, purified by centrifugation and dried.

Synthesis of hybrid (organic–inorganic) polymer-coated Janus particles

Preparation of colloidosomes and grafting of the PDMAEMA. Colloidosomes with 1000 nm large APTES-modified silica spheres were prepared by a wax–water Pickering emulsion approach described elsewhere.[50,51] The ATRP-initiator (α-bromoisobutyric acid) was then immobilized onto the exposed particle surface.[10] Subsequently, wax was dissolved in hexane, and partly initiator-covered particles were used for polymerization. PDMAEMA was grafted on the modified particles in the same manner as described above for the homogeneously coated particles at 70 °C for 120 min.

Grafting of PNIPAM. The "grafting to" approach was utilized to graft the second polymer onto the particles modified in the previous step (PDMAEMA/NH_2-JP). For this purpose, silica

particles with the grafted first polymer were dispersed in 25 mL of a 1 wt% carboxy terminated poly(N-isopropylacrylamide) (PNIPAM) solution in ethanol, and stirred for 2 hours. Next, the solvent was evaporated and the particles were annealed at 150 °C overnight. The ungrafted polymer chains were removed by multiple redispersion cycles of particles in appropriate solvents and subsequent centrifugation. As a result, bi-component 1000 nm-PDMAEMA/PNIPAM JPs were obtained.

Assembly experiments

Self-assembly experiments were carried out by mixing different mass ratios $M_{JP/PAA-HP}$ and numerical ratios $N_{JP/PAA-HP}$ of 1000-PDMAEMA/PNIPAM Janus particles (JP) with homogeneously PAA-covered particles (PAA-HP) (Table 1).

For a typical experiment, 1 mg mL^{-1} dispersions of particles of all sizes were prepared in filtered, aqueous KCl solution (1 or 10 mmol L^{-1}); pH 2, 6 and 9 were adjusted by addition of 0.1 M HCl or KOH. All dispersions were sonicated and stirred at 700 rpm for several hours under cooling to avoid crosslinking of the PDMAEMA shells. Then the particles were mixed in appropriate ratios by taking aliquots from the initial 1 mg mL^{-1} dispersions depending on the target structures. For the half-raspberry-like structures, the dispersion with 1000-PDMAEMA/PNIPAM-JP was dropwise slowly added to the dispersion of PAA-HP under continuous stirring. For the colloidal chains and clusters, vice versa, the dispersion of PAA-HP was dropwise slowly added to the dispersion of 1000-PDMAEMA/PNIPAM-JP. The resulting mixtures were diluted to 0.5 mg mL^{-1}, stirred at 700 rpm for one hour, and sonicated for 20 minutes. Samples for SEM and FLM imaging were taken at this point. In order to obtain individual micro-clusters in SEM and FLM, the mixtures were diluted five times and sonicated for 20 more minutes. For SEM, 5 µL droplets of the samples were placed on a silicon wafer and left to dry. For investigation of the pH-triggered reversibility, variation of the pH value was carried out under potentiometric control by addition of 0.1 M HCl or KOH. After adjustment of the pH value, the dispersions were stirred at 700 rpm for one hour and sonicated for 20 minutes before samples for SEM and FLM were taken again. For statistical analysis, 250 clusters taken from five samples at each pH value were counted via FLM. SEM images were always acquired to investigate the stability of the formed constructs in dry state.

A complete overview of the prepared samples using different particle size ratios $S_{JP/PAA-HP}$ is displayed in Table 1. The mass ratio $M_{JP/PAA-HP}$ was used as parameter for the preparation of the binary particle mixtures and describes the applied mass of JP per mass of PAA-HP. The numerical ratio $N_{JP/PAA-HP}$ describes the applied number of 1000-PDMAEMA/PNIPAM-JP per PAA-HP and was estimated using eqn (1):

$$N_{JP/PAA-HP} = \left(\frac{r}{R}\right)^3 M_{JP/PAA-HP} \qquad (1)$$

with R = radius of the large 1000-PDMAEMA/PNIPAM-JP and r = radius of the small PAA-HP.

Results and discussion

Synthesis and characterization of homogeneous and Janus particles

Synthesis of homogeneous (HP) and Janus (JP) polymer-modified core–shell particles. Negatively charged core–shell particles with homogeneous poly(acrylic acid) (PAA) shells (PAA-HP) were fabricated by grafting poly(tert-butyl acrylate) from the pre-modified silica core and subsequent hydrolysis (see Experimental section). The core diameters of the PAA-HP were varied from 200 nm to 650 nm (Table 2, Fig. S1a–c†). Homogeneously modified 1000 nm-particles with poly(2-dimethylaminoethyl methacrylate) (PDMAEMA) (HP) were also synthesized for reference experiments. 1000 nm large hairy Janus particles (JP) with positive charges on one hemisphere composed of poly(2-dimethylaminoethyl methacrylate) (PDMAEMA) and poly(N-isopropylacrylamide) (PNIPAM) polymer shells at the opposite sides (Fig. S1d†) were synthesized using a combined "grafting-from"/"grafting-to" approach as described elsewhere.[10,11,50,51] Briefly, silica particles, which had been premodified with amino silanes (APTES) (Fig. S2a†), were mixed with hot water and molten paraffin wax under vigorous stirring. Thus, wax droplets covered by APTES-modified silica particles, so-called colloidosomes, were formed (Fig. S2a†) and the particles were trapped at the wax–water interface (Fig. S2c†). The side of the silica particles, which was exposed to the water, was used for the immobilization of the ATRP initiator and, after wax removal, for
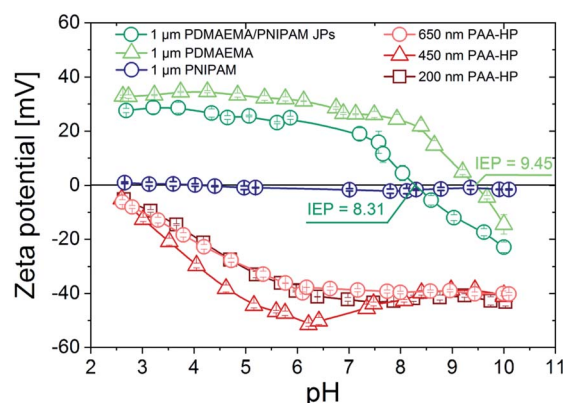
Table 1 Overview of the particle mixtures (PAA-HP and 1000-PDMAEMA/PNIPAM-JP) prepared for the self-assembly experiments, the mass ratio $M_{JP/PAA-HP}$ and the corresponding numerical ratio $N_{JP/PAA-HP}$

PAA-HP diameter [nm]	Particle size ratio $S_{JP/PAA-HP}$	1000-PDMAEMA/PNIPAM-JP : PAA-HP			
		Mass ratio $M_{JP/PAA-HP}$		Numerical ratio $N_{JP/PAA-HP}$	
200	5	1 : 4	100 : 1	1 : 500	4 : 5
450	2.2	1 : 4	15 : 1	1 : 44	4 : 3
650	1.5	1 : 4	15 : 1	1 : 15	4 : 1

Fig. 1 pH-dependent zeta potential of the synthesized PAA-HP (red) and PDMAEMA-HP and JP (green), as well as PNIPAM-HP as reference.

Table 2 List of the synthesized core–shell non-Janus (HP) and Janus particles (JP), their core and hydrodynamic diameters D, shell thicknesses H and isoelectric points (IEP). The core diameters were estimated based in SEM images of 40 unmodified silica core particles

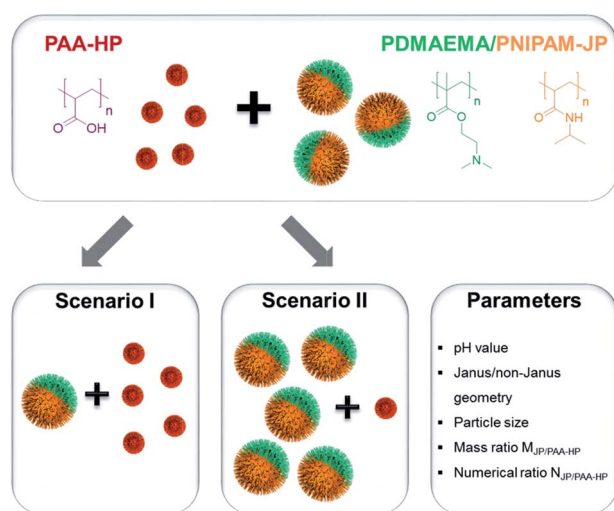| Sample ID	D^{core} (SEM) [nm]	$D_H^{core+shell}$	H^{dry} (TGA) [nm]	IEP
200-PAA-HP	208 ± 11	734	28	<2
450-PAA-HP	446 ± 18	940	14	<2
650-PAA-HP	639 ± 15	1203	19	<2
1000-PDMAEMA-HP	990 ± 23	1392	75	9.5
1000-PDMAEMA/PNIPAM-JP	990 ± 23	1385	42	8.3

Fig. 2 Two proposed scenarios for the assembly of binary mixtures of oppositely charged PAA-HP and 1000-PDMAEMA/PNIPAM-JP in dispersions. Varied parameters are: pH value, particle geometry (Janus and non-Janus), particle size, mass ratio $M_{JP/PAA-HP}$ and numerical ratio $N_{JP/PAA-HP}$.

grafting of PDMAEMA by ATRP (Fig. S2d†). Afterwards, the APTES-modified sides of the particles, which had been masked before, were used for attaching carboxy-terminated PNIPAM using the grafting-to approach. The Janus ratio of the particles is 2 : 1 (PDMAEMA : PNIPAM), which corresponds with the depth of the particle penetration into the wax phase during the colloidosome preparation process as described elsewhere (Fig. 2b and c).[52]

Design and characterization of dispersions. All synthesized particles were further characterized with scanning electron microscopy (SEM, Fig. S1 and S2†), dynamic light scattering (DLS), thermogravimetric analysis (TGA, Fig. S2e†) and electrophoretic measurements (Fig. 1 and S2f†). A complete overview of the particle samples with their diameters obtained from SEM images and DLS, polymer shell thicknesses obtained from TGA measurements and isoelectric points is displayed in Table 2. As observed in the SEM images, the polymer-decorated particles exhibit a slightly rough polymer morphology on their surface (Fig. S1†). The zeta potential of the polymer-modified particles as a function of pH was determined by measuring their electrophoretic mobility using electrophoresis (Fig. 1). The surface charge of the particles functionalized with acidic (PAA)

or basic (PDMAEMA) groups is highly dependent on the pH of the dispersion. Increasing pH causes an increase in the negative zeta potential in the case of PAA-modified particles due to the increased dissociation of the acidic carboxyl surface groups (Fig. 1, orange-red circles). The isoelectric point (IEP, pH value of zero charge) is at pH < 2. In the case of basic amino groups on PDMAEMA-containing JPs, the number of charges decreases with increasing pH due to their deprotonation (Fig. 1, green circles). The IEP of these particles is located at pH 8.3 (Table 2, Fig. 1). Nevertheless, there is a slight shift of the IEP value from 9.5 to 8.3 compared to homogeneously PDMAEMA-decorated particles due to the presence of uncharged PNIPAM hemispheres of the Janus particles. This indicates that both polymers are present on the Janus particle surface.[10,11]

The pH-responsive swelling behavior of PAA and PDMAEMA polymers grafted on silica particles was intensively studied in ref. 11. Briefly, the both used polymers exhibit an opposite swelling behavior (Fig. S3†). The PAA-modified particles are highly swollen at pH 9 due to the high negative charge density of PAA chains (swelling ratio is around 8), intermediately swollen at pH 6, and collapsed at pH 2 due to the absence of charges. Contrary, PDMAEMA polymer chains are protonated, highly charged and thus highly swollen at pH 2 (swelling ratio is around 5), intermediately stretched out at pH 6, and collapsed at pH 9. At pH 6 both polymers are in a charged and swollen state, which was set as starting pH value for all self-assembly experiments.

Starting from pH 6, the pH value was then adjusted to either pH 9 or pH 2, and backwards during five cycles in order to investigate the impact of the pH on the reversibility of self-assembled structures. To avoid interferences based on the increase of the ionic strength du, the ionic strength for all self-assembly experiments was adjusted with potassium chloride either to 1 (for half-raspberry-like structures) or 10 mmol L^{-1} (for cluster- and chain-like structures).

Analysis of formed structures and their reversibility

Two main scenarios were pursued for the self-assembly of binary mixtures of oppositely charged PAA-HP and 1000-PDMAEMA/PNIPAM-JP *via* electrostatic interactions to understand the shape of formed structures and their pH-triggered reversibility. In scenario I, an excess of smaller homogeneously modified particles was mixed with Janus particles of a larger size (Fig. 2, scenario I). Scenario II comprises the opposite situation, in which an excess of Janus particles with

a larger diameter was combined with smaller homogeneous particles (Fig. 2, scenario II). For the implementation of these two scenarios, we synthesized three types of particles: 200 nm, 450 nm and 650 nm homogeneously decorated with PAA (PAA-HP), 1000 nm large particles homogeneously decorated with PDMAEMA (PDMAEMA-HP, for reference purposes), and 1000 nm large Janus particles decorated with PDMAEMA and PNIPAM shells at their opposite sides (JP). The particles size ratio $S_{\text{JP/PAA-HP}} = D_{\text{JP}}/D_{\text{PAA-HP}}$ with D corresponding to the diameter of the silica core, the mass ratio $M_{\text{JP/PAA-HP}} = M_{\text{JP}}/M_{\text{PAA-HP}}$, and the numerical ratio $N_{\text{JP/PAA-HP}} = N_{\text{JP}}/N_{\text{PAA-HP}}$ ultimately determine the shape of the formed structure.
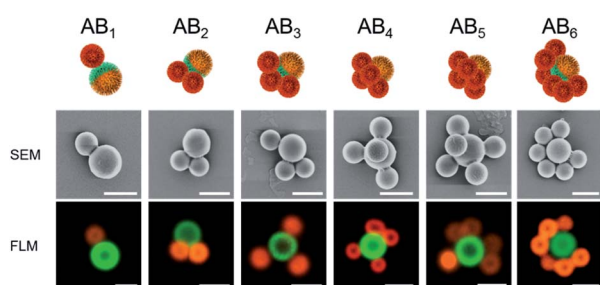

Fig. 3 Observed half-raspberry-like structures: schematic cartoons and representative SEM and FLM images obtained in dispersion of a mixture of non-Janus 650-PAA-HP and 1000-PDMAEMA/PNIPAM-JP (mass ratio $M_{\text{JP/PAA-HP}}$ 1 : 4, numerical ratio $N_{\text{JP/PAA-HP}}$ 1 : 15). FLM images were obtained with FITC and TRITC filters and the combined colors. The ionic strength was adjusted to 1 mmol L^{-1} with KCl. Scale bars: 1 μm.

(Half-)raspberry-like structures. First, we investigated the first scenario to study the assembly behavior between 1000-PDMAEMA/PNIPAM-JP and PAA-HP with an excess of PAA-HP, the geometry of formed structures, and their reversibility. The mass ratio $M_{\text{JP/PAA-HP}}$ was set to 1 : 4 (corresponds to numerical ratios $N_{\text{JP/PAA-HP}}$ of 1 : 500, 1 : 44 and 1 : 15 for 200-, 450- and 650-PAA-HP, respectively) and the appropriate particle size ratio $S_{\text{JP/PAA-HP}}$ was varied between 5.0 (for 200-PAA-HP), 2.2 (for 450-PAA-HP) and 1.5 (for 650-PAA-HP). In order to visualize the structures in dispersion, PAA-HP were modified with a red fluorescent dye (rhodamine) and PDMAEMA/PNIPAM-JPs with a green fluorescent dye (fluorescein) in the silica core during the Stöber process.

The formation of a wide range of AB_n-like structures by different numbers n of smaller PAA-HP (named as B) surrounding one larger PDMAEMA-decorated JP (named as A) was observed and visualized *via* FLM and SEM.

We observed raspberry-like (for non-Janus PDMAEMA-decorated particles, Fig. S4–S6†) and half-raspberry structures (for JP, exemplarily shown for 650-PAA-HP particles in Fig. 3). It should be noted that these structures were found both *in situ* in dispersion (FLM images, lower row in Fig. 3), and in dry state (SEM images, middle row in Fig. 3). Thus, drying effects did not seem to have any effect on the formation of the micro-structures. As anticipated, the degree of coverage is higher for non-Janus PDMAEMA particles compared to the Janus ones due to the spatially separated and, thus smaller, PDMAEMA areas on the Janus particles. Furthermore, we always observed a distri-bution of all AB_n-like structures (Fig. 3 and 4 left column), comprising dumbbell-like AB_1 up to half-raspberry AB_6
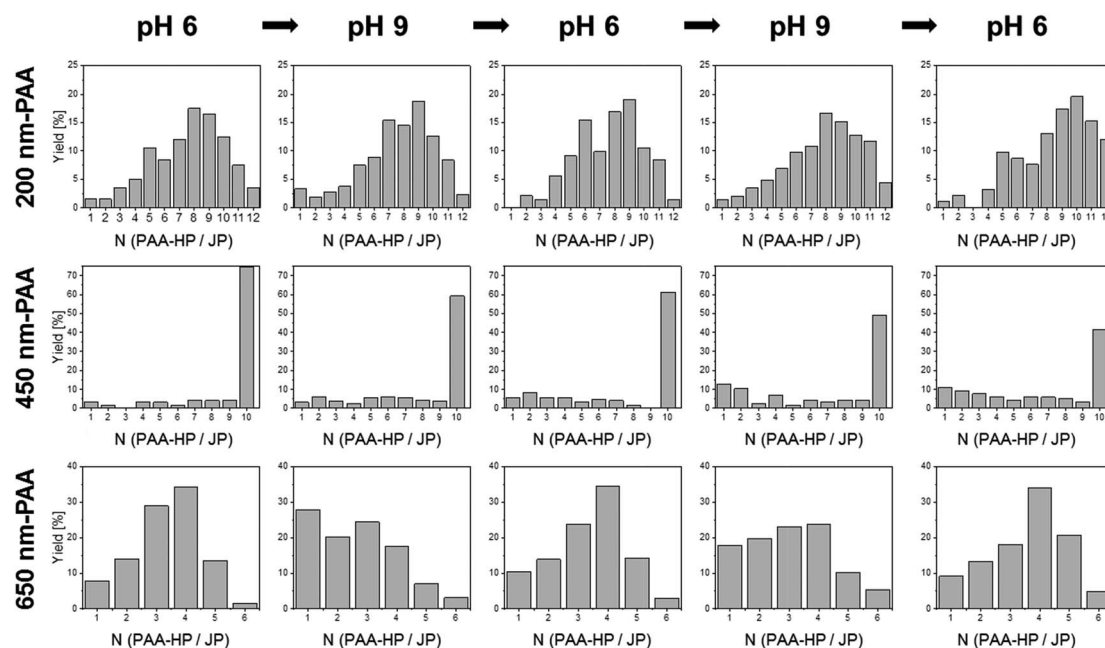

Fig. 4 Reversible self-assembly experiments: statistical analysis of the number of PAA-HP attaching to a single 1000-PDMAEMA/PNIPAM-JP (mass ratio $M_{\text{JP/PAA-HP}}$ 1 : 4; numerical ratios 1 : 500 for 200-PAA-HP, 1 : 44 for 450-PAA-HP, and 1 : 15 for 650-PAA-HP) forming a half-raspberry-like structure obtained from reversible pH switch from pH 6 to pH 9 and backwards. The ionic strength was adjusted to 1 mmol L^{-1} with KCl. 250 clusters were counted for each pH value, based on FLM images of five independent experiments.

structures. AB$_4$-like assemblies were found to be the predominant structure for this system with 650-PAA-HP ($\approx 35\%$ yield, Fig. 4 lowermost row).

AB$_n$-type half-raspberry constructs were also observed for higher particle size ratios $S_{JP/PAA-HP}$ of 2.2 (for 450-PAA-HP) and 5.0 (for 200-PAA-HP), which was realized using PAA-HP with larger diameters of 450 and 200 nm at a constant mass ratio $M_{JP/PAA-HP}$ of 1 : 4 (corresponds to $N_{JP/PAA-HP}$ of 1 : 44 for 450-PAA-HP and 1 : 500 for 200-PAA-HP). As expected, the maximum found number of PAA-HP attached to a single central JP increased with increasing particle size ratio (Fig. 4, left column).

For a more detailed quantification, the theoretically maximum number N_{max} of smaller PAA-HP in a hexagonal closed packing pattern on a single large JP was calculated as previously described in ref. 11 and 53 using eqn (2):

$$N_{max} = \frac{4}{3\left(1 - \dfrac{\sqrt{R^2 + 2Rr}}{R + r}\right)} \tag{2}$$

with R is the effective radius of the large JP and r is the effective radius of a small PAA-HP.

For this purpose, the effective radii of the particles were calculated either based on the polymer shell thicknesses H in dry state and the swelling ratio of the respective polymer *via* cryo-TEM[11] ($r_{cryo-TEM}$ and $R_{cryo-TEM}$), or *via* DLS measurements (r_{DLS} and R_{DLS}). R_{DLS} and r_{DLS} were calculated by 0.5 times $D_H^{core+shell}(DLS)$ (Table 3; see Table 2, third column for $D_H^{core+shell}(DLS)$). The effective radius $r_{cryo-TEM}$ is based on the swelling ratio (SR), which was determined *via* cryo-TEM to be 3 for PAA and 4 for PDMAEMA at neutral pH.[11] Thus, $r_{cryo-TEM}$ is calculated as follows:

$$r_{cryo-TEM} = 0.5 \cdot (H^{dry}(TGA)SR + d_H^{core}) \tag{3}$$

$H^{dry}(TGA)$ can be taken from Table 2, fourth column.

The experimentally obtained number of small HP on the surface of a large JP was compared with the maximum theoretical number (Table 3, Fig. 5).

The theoretical results show that the number of PAA-HP on a single JP decreases when increasing the PAA-particle size (Fig. 5), which is in reasonable agreement with the results from ref. 11. However, much lower numbers of PAA-HP attached to one single JP were found in the DLS and cryo-TEM experiments compared to the theoretical results in accordance with further
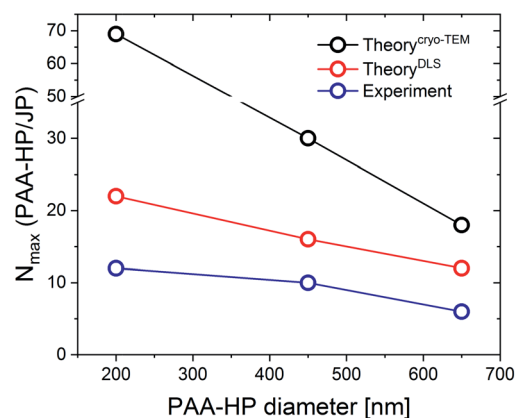

Fig. 5 Comparison of the theoretical and experimental numbers N of PAA-HP on a single JP depending on the PAA particle size.

investigations.[11] In the experiments, hexagonal close packing could be hindered by the repulsive forces between two neighboring PAA-HP carrying similar negative charges, which leads to empty spaces between the PAA-HP.[11] On the contrary, the theoretical model does not consider charges of the colloids and resulting attraction or repulsion between them at all. Generally, theoretical results determined with effective radii from DLS measurements (Fig. 5, red line) correspond better with the experimental findings (Fig. 5, blue line) than the theoretical results obtained *via* cryo-TEM (Fig. 5, black line). We assume that the hydrodynamic radius obtained from DLS measurements represents a more realistic value for the determination of the size of a polyelectrolyte-decorated particle.

Reversibility of formed (half-)raspberry-like structures. We varied the pH value from pH 6 to pH 9 and backwards. Decreasing the pH down to 2 led to strong aggregation of the PAA-modified particles in this pH region, which is close to the IEP of PAA, and was therefore not further investigated. A detailed protocol for the realization of the reversibility experiments can be found in the Experimental part. Fig. 4 displays the statistical analysis of the formed structures for PAA-HP particles of different diameters (200 nm, 450 nm, and 650 nm) attaching to a single 1000-PDMAEMA/PNIPAM-JP. We observed that structures created by 650-PAA-HP particles and 1000-PDMAEMA/PNIPAM-JP showed a remarkable reversibility. At the starting pH value of 6, AB$_4$ structures were preferred due to the strong electrostatic attraction between negatively charged 650-PAA-HP and positively charged 1000-PDMAEMA/PNIPAM-JP

Table 3   Theoretically maximum number (N^{Theory}) and experimentally obtained maximum number ($N^{Experiment}$) of the small PAA–HP on a single large PDMAEMA/PNIPAM-JP. N^{Theory} were determined based on the effective radii obtained from both cryo-TEM and DLS

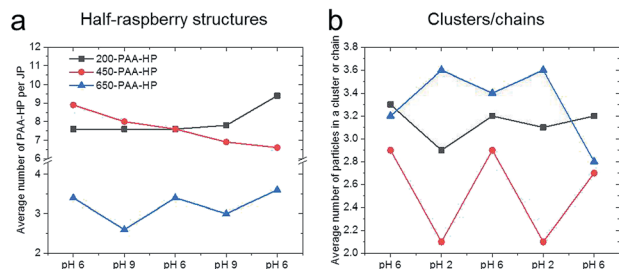| PAA system	Effective radius r [nm]		N_{max}^{Theory}		$N_{max}^{Experiment}$
	Cryo-TEM	DLS	Cryo-TEM	DLS	
200-PAA-HP	142	367	69	22	12
450-PAA-HP	246	470	30	16	10
650-PAA-HP	354	602	18	12	6
1000-PDMAEMA/PNIPAM-JP	584	693	—	—	—

Fig. 6 (a) Average number of 200-, 450- and 650-PAA-HP on a single 1000-PDMAEMA/PNIPAM-JP forming a half-raspberry-like assembly at pH 6 and pH 9. (b) Average number of particles (200-, 450- or 650-PAA-HP and 1000-PDMAEMA/PNIPAM-JP) forming a cluster or chain-like structure at pH 6 and pH 2.

in this pH regime (Fig. 1, 3, and 4). After increasing the pH up to 9, PDMAEMA polymer chains lose their positive charge (Fig. 1, dark green curve) due to the deprotonation effect inducing a weaker attraction to the 650-PAA-HP particles. This results in favored AB_1 structures (one 650-PAA-HP attached to one JP). This tendency can be reversed by decreasing the pH value back to 6, where PDMAEMA gained its positive charge again and AB_4 structures were again preferred. To further quantify the reversibility of the assembly process, the average number of PAA-HP attached to a single 1000-PDMAEMA/PNIPAM-JP forming a half-raspberry structure was calculated and is displayed in Fig. 6a (blue curve) and Table S1.† The average number of 650-PAA-HP on a single JP reversibly de- and increases by roughly 20% when changing the pH from 6 to 9 and backwards, respectively. A similar effect as described above was found by Kegel et al. in 2017, who showed that the pH value offers an experimental knob to adjust the charge density of polyelectrolytes and, thus, the electrostatic interactions between two oppositely charged non-Janus colloids. The surface coverage of a large positively charged colloid by smaller negatively charged colloids could be increased when decreasing the pH.[38]

Contrary, reversibility of structures made of 200-PAA-HP or 450-PAA-HP and 1000-PDMAEMA/PNIPAM-JP could not be observed at all (Fig. 4 and 6a). We assume that the found tendencies are caused by geometrical and electrostatic effects. Indeed, all sizes of PAA-modified are attached to the PDMAEMA shell of the central 1000-PDMAEMA/PNIPAM-JP due to their opposite charges. But when the PAA-particles are small compared to the central JP (<650 nm), they are spatially enclosed and locked by electrostatics and/or entanglements ("caging") with the PDMAEMA polymer chains to a larger extent. The extensive three-dimensional enveloping of small PAA-particles in the PDMAEMA shell of the JPs hinders their release from the central 1000-PDMAEMA/PNIPAM-JP even after pH increase. Thus, the dense packing of the smaller particles is irreversible. The stability of assembled structures can be compared with polyelectrolyte multilayers fabricated e.g. via layer-by-layer processes,[54,55] which are thermodynamically stable structures. Molecular-dynamics simulation also showed that the polyelectrolyte multilayers are "fuzzy" and the

molecules of one layer interpenetrate other layers.[56] Spruijt and coworkers reported a similar effect on polymer brush-modified colloidal particles. They presented systems consisting of oppositely charged colloidal particles, which assembled into large clusters, and disassembled when increasing the salt concentration. They found that interparticle interactions are governed by a time-dependent attractive electrostatic complexation that strengthens in time due to interpenetration of the polymer brushes.[12] Indeed, the average value of 200-PAA-HP per 1000-PDMAEMA/PNIPAM-JP forming half-raspberry-like assemblies slightly increases with proceeding cycle number (Fig. 6a, black curve), which seemed to hint at strengthening electrostatic complexation in time as described by Spruijt et al. However, an opposite tendency was found for 450-PAA-HP: less 450-PAA-HP attached to a single Janus particle with increasing cycle number (Fig. 6a, red curve). Therefore, we assume that not only electrostatic, but particularly geometrical "caging" effects may have an effect on the irreversibility of assemblies. Small 200-PAA-HP could be easily and irreversibly caged in the shell of the Janus particles, while medium-sized 450-PAA-HP were released in time despite almost constant ionic strength because of weaker "caging" effects. Only 650-PAA-HP are large enough that neither "caging" nor ionic effects occurred, which enabled the reversibility of the system.

Maas et al. investigated the influence of the particle size on the assembled constructs, and reported that the use of small particles in assembly processes of binary particle mixtures leads to uncontrolled aggregation, bridging of the particles and high polydispersity of the formed structures.[57] They hypothesize that this phenomenon is not governed by kinetics, but rather by aggregation of the small particles within the ion cloud of the central particles, when the adsorbing particle is small compared to the diameter of the ion cloud.[57] Based on this hypothesis, we cannot disprove that the effect of aggregation of small particles within the ion cloud of the central particles also occurs for 200-PAA-HP due to the broad distribution of observed AB_n structures. 450-PAA-HP show a more narrow distribution of the AB_n structures probably due to the more controlled aggregation within the ion cloud of the 1000-PDMAEMA/PNIPAM-JP. However, all PAA-HP appeared to randomly attach at the PDMAEMA-hemisphere of the 1000-PDMAEMA/PNIPAM-JP and rather not with the maximum distance to each other because of the neutralization of the PAA chains in the PDMAEMA ion cloud.

Colloidal clusters. A wide range of colloidal clusters were observed by increasing the mass ratio $M_{JP/PAA-HP}$ up to 15 : 1 for 450- and 650-PAA-HP and 100 : 1 for 200-PAA-HP (corresponds to numerical ratios $N_{JP/PAA-HP}$ to 4 : 5 for 200-PAA-HP, 4 : 3 for 450-PAA-HP, and 4 : 1 for 650-PAA-HP) and are exemplarily shown for 650-PAA-HP and JPs in Fig. 7a. In order to quantify the self-assembly result, we counted the number of particles forming A_nB structures consisting of different numbers n of larger JP A and smaller PAA-HP B (obtained from FLM images). The scope of structures ranges from dumbbell-like structures, such as A_1B, to flower-like constructs, such as A_5B or A_6B.

Furthermore, the particle size ratio $S_{JP/PAA-HP}$ seemed to have an impact on the size of the clusters. An increase of the particle
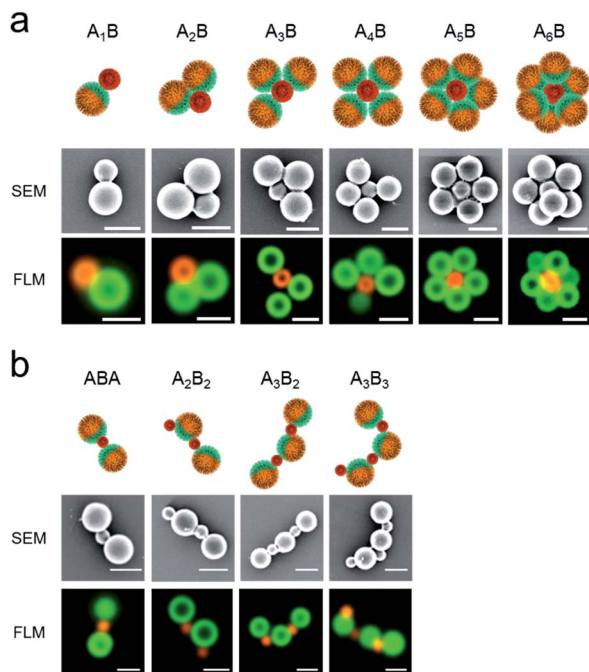
Fig. 7 Observed colloidal clusters and colloidal chains. (a) Schematic and representative SEM and FLM images of colloidal clusters, formed in dispersion from 1000-PDMAEMA-PNIPAM-JP and 650-PAA-HP (mass ratio $M_{JP/PAA-HP}$ 15 : 1, numerical ratio $N_{JP/PAA-HP}$ 4 : 1). (b) Schematic and representative SEM and fluorescence microscopy images of colloidal chains, formed in dispersion from 1000-PDMAEMA-PNIPAM-JP and 450-PAA-HP (mass ratio $M_{JP/PAA-HP}$ 15 : 1, numerical ratio $N_{JP/PAA-HP}$ 4 : 3). FLM images were obtained with different filters and the combined colors. The ionic strength was adjusted to 10 mmol L^{-1} with KCl. Scale bars: 1 μm.
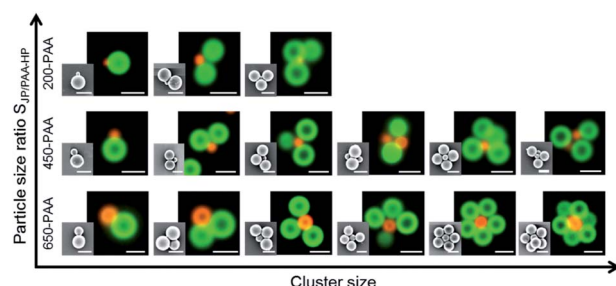

Fig. 8 Phase diagram with representative SEM and FLM images of colloidal clusters formed during the self-assembly of PAA-HP (diameter varied between 200 nm, 450 nm and 650 nm) and 1000-PDMAEMA/PNIPAM-JP (constant diameter of 1000 nm; mass ratio $M_{JP/PAA-HP}$ 15 : 1, numerical ratios $N_{JP/PAA-HP}$ 4 : 5, 4 : 3 and 4 : 1, respectively); the cluster size decreases with increasing particle size ratio $S_{JP/PAA-HP}$. Scale bar: 1 μm. x-axis: geometry/shape and size of formed clusters; y-axis: particle size ratio $S_{JP/PAA-HP}$.

size ratio $S_{JP/PAA-HP}$ resulted in a decrease of the occurring cluster size (Fig. 8). A small central 200-PAA-HP enables the formation of clusters consisting of maximum four particles due to the steric hindrance and fast charge compensation. The small surface of the 200-PAA-HP leads also to small distances between the partly positively charged JP, which leads to
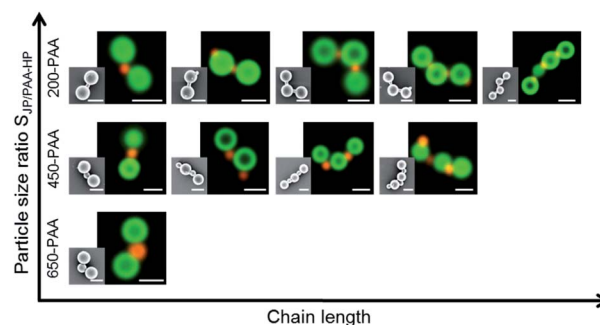

Fig. 9 Diagram with representative SEM and FLM images of the colloidal chains formed during the self-assembly of PAA-HP and 1000-PDMAEMA/PNIPAM-JP (mass ratio $M_{JP/PAA-HP}$ 15 : 1, numerical ratios $N_{JP/PAA-HP}$ 4 : 5, 4 : 3 and 4 : 1, respectively); the chain length increases with increasing particle size ratio $S_{JP/PAA-HP}$. Scale bar: 1 μm. x-axis: geometry/shape and size of formed chains; y-axis: particle size ratio $S_{JP/PAA-HP}$.

repulsive electrostatic forces between them, and hinders the attachment of further JP to the central 200-PAA-HP. Larger central PAA-HP provide a larger surface and a higher number of negative charges per PAA particle, thus more partly positively charged JPs can be included in a cluster.

Colloidal chains. In analogy to the cluster structures described above, colloidal chains were observed by increasing the mass ratio $M_{JP/PAA-HP}$ up to 15 : 1 (corresponds to numerical ratios $N_{JP/PAA-HP}$ to 4 : 5 for 200-PAA-HP, 4 : 3 for 450-PAA-HP, and 4 : 1 for 650-PAA-HP) and are exemplarily summarized for 450-PAA-HP and JP in Fig. 7b and 9. Although colloidal clusters and colloidal chains emerge simultaneously at this mass ratio, the formation of colloidal clusters is favored over colloidal chains in general (Fig. 10). Similar structures and tendencies were shown by Kraft et al., who also obtained a mixture of chain-like (colloidal polymer) and cluster structures (colloidal molecules) made of DNA linker-modified particles at particle size ratio of 2 : 1. The percentage of the formed structures could be also programmed by controlling the mixing ratio.[43]

The length of A_nB_m-like chains exhibits a dependency on the particle size ratio $S_{JP/PAA-HP}$ (Fig. 9), which is, interestingly, opposite to the tendency found for clusters (cf. Fig. 8): the higher the particle size ratio $S_{JP/PAA-HP}$, the higher the length of the formed chains (Fig. 9). The formation of colloidal chains is preferred for smaller PAA-HP (200 nm and 450 nm), while the formation of clusters is preferred for larger connecting PAA-HP. It means the smaller the size of the "connecting" PAA-HP, the higher is the probability to form longer chains. This tendency can be explained with the increasing numerical ratio $N_{JP/PAA-HP}$ when increasing the particle size ratio $S_{JP/PAA-HP}$ (Table 1). That means that with increasing diameter of the PAA-HP the number of available PAA-HP per 1000-PDMAEMA/PNIPAM-JP decreases, which reduces the probability to form longer colloidal chains declines. Furthermore, the observed trend is probably supported by steric matters: smaller PAA-HP hamper the attachment of more than two large JP to form a cluster, which facilitates the formation of colloidal chains.
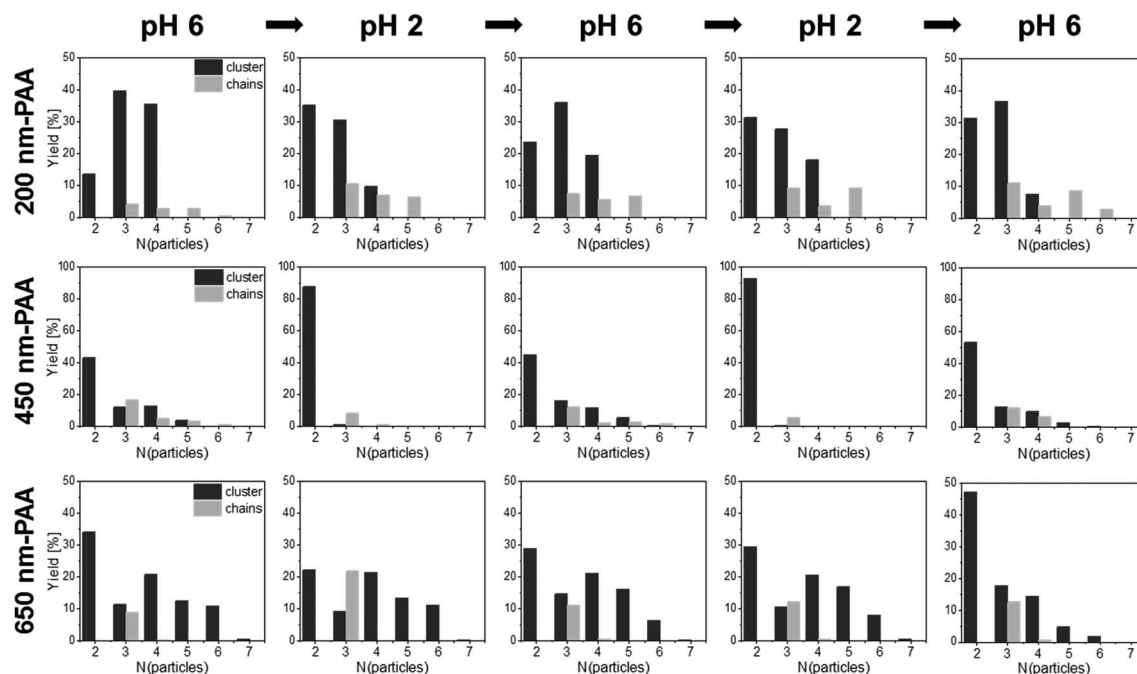
Fig. 10 Reversible self-assembly experiments: statistical analysis of the number of PAA–HP and 1000–PDMAEMA–PNIPAM JP (mass ratio $M_{JP/PAA-HP}$ 15 : 1, numerical ratios $N_{JP/PAA-HP}$ 4 : 5, 4 : 3 and 4 : 1, respectively) forming a colloidal cluster or a colloidal chain obtained from reversible pH switch from pH 6 to pH 2 and backwards. The ionic strength was adjusted to 10 mmol L^{-1} with KCl. 250 clusters were counted for each pH value, based on FLM images of five independent experiments.

Reversibility of colloidal clusters and chains. In order to investigate the reversibility of the formation of clusters and colloidal chains, we varied the pH value from pH 6 to 2 and backwards. An increase to pH 9 was not relevant due to the high aggregation tendency of the JP at pH values above the IEP of PDMAEMA. Fig. 10 displays the statistical analysis of the formed colloidal clusters and colloidal chains. As already explained above, the formation of clusters is generally preferred over the formation of colloidal chains for all sizes of PAA-HP and all pH values. An increase of the PAA-HP size to 650 nm leads to larger clusters, while the formation of longer chains is preferred for smaller 450- and 200-PAA-HP.

The most pronounced reversibility was observed for 450-PAA-HP and 1000-PDMAEMA/PNIPAM-JPs for both clusters and colloidal chains (Fig. 6b, Tables S2–S4†). At pH 6, larger clusters and chains comprising three, four or five particles were present (due to electrostatic interactions between oppositely charged PAA-HP and JP) although the number of A_1B clusters was predominant (average number of particles forming a cluster or chain is 2.9; Fig. 6b, Table S4†). A decrease of the pH value down to pH 2 (close to the IEP of PAA) caused a loss of negative charges in the PAA polymer chains resulting in a weak electrostatic attraction to the JPs. Thus, the yield of longer chains and larger clusters is reduced at pH 2, and the average number of particles forming a cluster or chain decreases by 28% from 2.9 to 2.1 (Fig. 6b, Table S4†). This tendency can be inverted multiple times by increasing and re-decreasing the pH value (Fig. 6b). This dynamic reversibility determined by pH is also discernible for 200-PAA-HP and 650-PAA-HP even though the effect was not as pronounced as for 450-PAA (Fig. 6b, Tables S2–S4†).

Conclusions

In summary, we investigated the pH-triggered reconfigurable assembly of structures composed of binary mixtures of poly(2-dimethylamino)ethyl methacrylate (PDMAEMA)/poly(N-iso-propylacrylamide) (PNIPAM) Janus and polyacrylic acid (PAA)-decorated non-Janus particles. We found that the particle size ratio $S_{JP/PAA-HP}$ and the numerical ratio $N_{JP/PAA-HP}$ strongly determine the geometry of the obtained constructs as well as the quality of the reversibility of the assembly process. The formed structures are well-defined and stable in a certain pH range. The structures also have the advantage that the particle interactions are bistable. They can be disassembled on demand by changing the pH value, and then reassembled into new stable structures many times. Specifically, half-raspberry-like assemblies with a higher number of smaller PAA-particles attached to the larger central JPs are formed at pH 6 due to strong electrostatic interactions and at a mass ratio $M_{JP/PAA-HP}$ of 1 : 4 (corresponding numerical ratios $N_{JP/PAA-HP}$ of 1 : 500 for 200-PAA-HP, 1 : 44 for 450-PAA-HP, and 1 : 15 for 650-PAA-HP). However, only binary particle mixtures with a particle size ratio $S_{JP/PAA-HP}$ of 2.2 could be reversibly disassembled when the pH is increased close to the IEP of the PDMAEMA polymer chains causing weakened attraction between the particles.

Both colloidal clusters and chains are formed at a mass ratio $M_{JP/PAA-HP}$ of 15 : 1 (corresponding numerical ratios $N_{JP/PAA-HP}$ of 4 : 5 for 200-PAA-HP, 4 : 3 for 450-PAA-HP, and 4 : 1 for 650-PAA-HP). The formation of clusters was generally preferred over the formation of colloidal chains for all sizes of PAA-HP and all pH values. The particle size ratio $S_{JP/PAA-HP}$ strongly determined the

size of the formed colloidal clusters: an increase of $S_{\text{JP/PAA-HP}}$ decreased the size of the formed clusters. Colloidal clusters could also be reversibly reassembled to chain-like structures (preferably of A_1B-type) by decreasing the pH to 2 which is close to the IEP of the PAA-decorated particles. However, colloidal chains, although they were observed at the same mass ratio $M_{\text{JP/PAA-HP}}$ and numerical ratio $N_{\text{JP/PAA-HP}}$ like colloidal clusters, exhibited the opposite dependency on the particle size ratio $S_{\text{JP/PAA-HP}}$ compared to colloidal clusters: by increasing the particle size ratio $S_{\text{JP/PAA-HP}}$, the length of the colloidal chains could be increased.

The presented approach provides new insight into the topic of reconfigurable self-assembly of particles with surface polymer patches into colloidal superstructures with controlled shapes. This may open up a variety of self-assembly-based applications towards miniaturization of machines, catalysis, photonics/plasmonics, photovoltaics, or nanoscale electronics.

Conflicts of interest

There are no conflicts to declare.

Acknowledgements

References

1 J. Zhang, J. Yan and S. Granick, *Angew. Chem., Int. Ed. Engl.*, 2016, **55**, 5166–5169.

2 J. Yan, M. Han, J. Zhang, C. Xu, E. Luijten and S. Granick, *Nat. Mater.*, 2016, **15**, 1095–1099.

3 W. Gao, A. Pei, X. Feng, C. Hennessy and J. Wang, *J. Am. Chem. Soc.*, 2013, **135**, 998–1001.

4 F. Li, D. P. Josephson and A. Stein, *Angew. Chem., Int. Ed. Engl.*, 2011, **50**, 360–388.

5 M. Vallet-Regi, *Chemistry*, 2006, **12**, 5934–5943.

6 J. A. Melero, R. van Grieken and G. Morales, *Chem. Rev.*, 2006, **106**, 3790–3812.

7 K. Hou, B. Tian, F. Li, Z. Bian, D. Zhao and C. Huang, *J. Mater. Chem.*, 2005, **15**, 2414–2420.

8 Y. Gao and Y. Yu, *J. Am. Chem. Soc.*, 2013, **135**, 19091–19094.

9 P. Johal and S. Chaudhary, *International Journal of Advances in Engineering Sciences and Applied Mathematics*, 2013, **2**, 106–110.

10 A. Kirillova, G. Stoychev, L. Ionov and A. Synytska, *Langmuir*, 2014, **30**, 12765–12774.

11 A. Kirillova, G. Stoychev and A. Synytska, *Faraday Discuss.*, 2016, **191**, 89–104.

12 E. Spruijt, H. E. Bakker, T. E. Kodger, J. Sprakel, M. A. Cohen Stuart and J. van der Gucht, *Soft Matter*, 2011, **7**, 8281–8290.

13 M. E. Leunissen, C. G. Christova, A. P. Hynninen, C. P. Royall, A. I. Campbell, A. Imhof, M. Dijkstra, R. van Roij and A. van Blaaderen, *Nature*, 2005, **437**, 235–240.

14 A. M. Mihut, B. Stenqvist, M. Lund, P. Schurtenberger and J. J. Crassous, *Sci. Adv.*, 2017, **3**, e1700321.

15 Q. Chen, J. K. Whitmer, S. Jiang, S. C. Bae, E. Luijten and S. Granick, *Science*, 2011, **331**, 199–202.

16 D. J. Kraft, R. Ni, F. Smallenburg, M. Hermes, K. Yoon, D. A. Weitz, A. van Blaaderen, J. Groenewold, M. Dijkstra and W. K. Kegel, *Proc. Natl. Acad. Sci. U. S. A.*, 2012, **109**, 10787–10792.

17 S. Asakura and F. Oosawa, *J. Polym. Sci.*, 1958, **33**, 183–192.

18 S. Gangwal, O. J. Cayre and O. D. Velev, *Langmuir*, 2008, **24**, 13312–13320.

19 S. Gangwal, A. Pawar, I. Kretzschmar and O. D. Velev, *Soft Matter*, 2010, **6**, 1413–1418.

20 K. L. Heatley, F. Ma and N. Wu, *Soft Matter*, 2017, **13**, 436–444.

21 Q. Chen, E. Diesel, J. K. Whitmer, S. C. Bae, E. Luijten and S. Granick, *J. Am. Chem. Soc.*, 2011, **133**, 7725–7727.

22 S. K. Smoukov, S. Gangwal, M. Marquez and O. D. Velev, *Soft Matter*, 2009, **5**, 1285–1292.

23 J. Yan, M. Bloom, S. C. Bae, E. Luijten and S. Granick, *Nature*, 2012, **491**, 578–581.

24 K. P. Yuet, D. K. Hwang, R. Haghgooie and P. S. Doyle, *Langmuir*, 2010, **26**, 4281–4287.

25 J. Yan, S. C. Bae and S. Granick, *Adv. Mater.*, 2015, **27**, 874–879.

26 A. Nikoubashman, *Soft Matter*, 2016, **13**, 222–229.

27 Y. Abe, B. Zhang, L. Gordillo, A. M. Karim, L. F. Francis and X. Cheng, *Soft Matter*, 2017, **13**, 1681–1692.

28 A. F. Demirors, P. P. Pillai, B. Kowalczyk and B. A. Grzybowski, *Nature*, 2013, **503**, 99–103.

29 J. Zhang and S. Granick, *Faraday Discuss.*, 2016, **191**, 35–46.

30 A. M. Percebom, J. J. Giner-Casares, N. Claes, S. Bals, W. Loh and L. M. Liz-Marzan, *Chem. Commun.*, 2016, **52**, 4278–4281.

31 G. M. Whitesides and B. Grzybowski, *Science*, 2002, **295**, 2418–2421.

32 N. Krasnogor, S. Gustafson, D. A. Pelta and J. L. Verdegay, *Systems Self-Assembly: Multidisciplinary Snapshots*, Elsevier, Amsterdam, 2008.

33 Y. Wang, G. Chen, M. Yang, G. Silber, S. Xing, L. H. Tan, F. Wang, Y. Feng, X. Liu, S. Li and H. Chen, *Nat. Commun.*, 2010, **1**, 87.

34 Y. Liu, X. Han, L. He and Y. Yin, *Angew. Chem., Int. Ed. Engl.*, 2012, **51**, 6373–6377.

35 C. Rossner, O. Glatter and P. Vana, *Macromolecules*, 2017, **50**, 7344–7350.

36 C. Rossner, Q. Tang, O. Glatter, M. Muller and P. Vana, *Langmuir*, 2017, **33**, 2017–2026.

37 Z. Tian, C. Yang, W. Wang and Z. Yuan, *ACS Appl. Mater. Interfaces*, 2014, **6**, 17865–17876.

38 Y. Guo, B. G. P. van Ravensteijn, C. H. J. Evers and W. K. Kegel, *Langmuir*, 2017, **33**, 4551–4558.

39 Z. Sun, W. Ni, Z. Yang, X. Kou, L. Li and J. Wang, *Small*, 2008, **4**, 1287–1292.

40 M. Grzelczak and L. M. Liz-Marzan, *J. Phys. Chem. Lett.*, 2014, **5**, 2455–2463.

41 T. Lee, K. Gizynski and B. A. Grzybowski, *Adv. Mater.*, 2017, **29**, 1704274.

42 B. A. Grzybowski, K. Fitzner, J. Paczesny and S. Granick, *Chem. Soc. Rev.*, 2017, **46**, 5647–5678.

43 I. Chakraborty, V. Meester, C. van der Wel and D. J. Kraft, *Nanoscale*, 2017, **9**, 7814–7821.

44 S. Wintzheimer, T. Granath, M. Oppmann, T. Kister, T. Thai, T. Kraus, N. Vogel and K. Mandel, *ACS Nano*, 2018, **12**, 5093–5120.

45 B. Bharti, D. Rutkowski, K. Han, A. U. Kumar, C. K. Hall and O. D. Velev, *J. Am. Chem. Soc.*, 2016, **138**, 14948–14953.

46 Q. Chen, S. C. Bae and S. Granick, *J. Am. Chem. Soc.*, 2012, **134**, 11080–11083.

47 C. Yu, J. Zhang and S. Granick, *Angew. Chem., Int. Ed. Engl.*, 2014, **53**, 4364–4367.

48 J. Yan, S. C. Bae and S. Granick, *Soft Matter*, 2015, **11**, 147–153.

49 Q. Zhang, R. Dong, X. Chang, B. Ren and Z. Tong, *ACS Appl. Mater. Interfaces*, 2015, **7**, 24585–24591.

50 S. Berger, A. Synytska, L. Ionov, K.-J. Eichhorn and M. Stamm, *Macromolecules*, 2008, **41**, 9669–9676.

51 S. Berger, L. Ionov and A. Synytska, *Adv. Funct. Mater.*, 2011, **21**, 2338–2344.

52 A. Synytska, A. Kirillova and L. Isa, *ChemPlusChem*, 2014, **79**, 656–661.

53 H. Xing, Z. Wang, Z. Xu, N. Y. Wong, Y. Xiang, G. L. Liu and Y. Lu, *ACS Nano*, 2012, **6**, 802–809.

54 M. Müller, B. Urban and S. Schwarz, *Langmuir*, 2018, **34**, 8129–8144.

55 J. J. Richardson, J. Cui, M. Bjornmalm, J. A. Braunger, H. Ejima and F. Caruso, *Chem. Rev.*, 2016, **116**, 14828–14867.

56 B. Abu-Sharkh, *J. Chem. Phys.*, 2005, **123**, 114907.

57 M. Maas, C. C. Silverio, J. Laube and K. Rezwan, *J. Colloid Interface Sci.*, 2017, **501**, 256–266.